Journal of Solid State Chemistry **149,** 354–359 (2000)
doi:10.1006/jssc.1999.8544, available online at http://www.idealibrary.com on IDEAL®

Synthesis and Magnetic Properties of $Ln_{2/3}TiO_3$ (Ln = Pr and Nd)

K. Yoshii

Department of Synchrotron Radiation Research, Japan Atomic Energy Research Institute (JAERI), Mikazuki, Hyogo 679-5148, Japan
E-mail: yoshiike@spring8.or.jp

Received June 23, 1999; in revised form October 4, 1999; accepted October 22, 1999

The *A*-site-deficient perovskite compounds $Ln_{2/3}TiO_3$ with Ln = Pr and Nd were synthesized under an H_2–Ar atmosphere at 1400 and 1450°C, respectively. The samples were found to have slight oxygen deficiencies of $\delta \sim 0.006$ in $Ln_{2/3}TiO_{3-\delta}$. It was also found that no single-phase compound could be prepared in air from the same initial mixtures. Their crystal structures were assigned to a double perovskite structure with the orthorhombic space group *Pmmm*, as in the case of $La_{2/3}TiO_3$. In both systems, no obvious magnetic ordering was observed between 2 and 300 K in susceptibility–temperature (χ–T) curves. Inverse susceptibility–temperature ($1/\chi$–T) curves were found to deviate from the Curie–Weiss law below ~30 and ~90 K for $Pr_{2/3}TiO_3$ and $Nd_{2/3}TiO_3$, respectively. Magnetization–field (M–H) curves exhibited paramagnetic profiles for $Pr_{2/3}TiO_3$ down to 2 K and a tendency toward magnetic ordering for $Nd_{2/3}TiO_3$ at 2 K.

1. INTRODUCTION

It is known that perovskite compounds with the formula AMO_3 can tolerate wide-range A-site deficiencies in some system (A, alkaline metals, alkaline earth metals, or lanthanides; M, transition metals) such as $Na_{1-x}WO_3$ ($x \leqq 0.7$) (1) and $Sr_{1-x}NbO_3$ ($x \leqq 0.3$) (2). In several compounds with the formula $A_{1/3}MO_3$ (3,4), two-thirds of the A-site ions are vacant (A, lanthanides; M, Nb and Ta). The vacancies settle into an ordered arrangement, leading to a double perovskite structure with a doubled periodicity along the c axis.

$La_{2/3}TiO_3$ is the compound where one-third of the A-site La ions are vacant (5–7). While no La-deficient system $LaTiO_3$ is a so-called Mott–Hubbard type insulator which has a Ti^{3+} ($3d^1$) localized spin ($S = 1/2$) on each Ti site (8), this compound is a band insulator because of the diamagnetic Ti^{4+} ($3d^0$) ions. Its crystal structure is essentially the same as that of $La_{1/3}NbO_3$ (5). Due to the crystallographic ordering of the A-site vacancy, the system also has a double perovskite structure (5–7). Its detailed properties were investigated for a slightly oxygen-deficient phase $La_{2/3}TiO_{3-\delta}$ (6). It was found that the crystal structure for $\delta \leq 0.046$ is orthorhombic *Pmmm*, while the structure is tetragonal *P*4/*mmm* for $\delta \geq 0.046$. Furthermore, lightly oxygen-deficient samples with a 3*d* electron density lower than 0.33 showed semiconductive behavior, while higher oxygen deficient samples were metallic. The single crystals of this compound were also synthesized with the flux growth method, and their growth conditions, crystal structure, crystal morphology, and dielectric properties were investigated (7).

To the author's knowledge, detailed properties for $Ln_{2/3}TiO_3$ containing heavier lanthanide (Ln) ions have not been reported so far. In this work, of these compounds, $Pr_{2/3}TiO_3$ and $Nd_{2/3}TiO_3$ were synthesized, containing magnetic Ln ions Pr^{3+} ($4f^2$) and Nd^{3+} ($4f^3$), and their crystallographic and magnetic properties were investigated.

2. EXPERIMENTAL

The samples were prepared by the ceramic method. They were prepared twice, and its was confirmed that they showed reproducible structural and magnetic properties. The starting materials, as-cast Pr_2O_3 (3 N, Soekawa), dried Nd_2O_3 (4N, Soekawa), and TiO_2 (4 N, Soekawa), were weighed following the reaction

$$(1/3)Ln_2O_3 + TiO_2 \rightarrow Ln_{2/3}TiO_3 \ (Ln = \text{Pr and Nd}).$$

The starting mixtures were well ground, pressed into pellets, and fired in an H_2–Ar flow (H_2 5% and purity 5N) or in air for 10 h up to 1450°C. The cooling rate down to room temperature was 100°C/hr. The firing was repeated twice. As shown below, single-phase samples were prepared only in the H_2–Ar flow. Their crystal structures were determined by powder XRD (X-ray diffraction) measurements using Cu$K\alpha$ radiation (MAC Science Co., M03XHF^{22}). The XRD patterns were analyzed by the Rietveld method using the program RIETAN (9). For the single-phase samples, the oxygen contents were determined by the TGA (thermogravimetric analysis) method when they were heated up to 1100°C in air (Rigaku TAS200). They were found to have slight oxygen deficiencies δ in $Ln_{2/3}TiO_{3-\delta}$ of 0.006, with

0022-4596/00 $35.00

experimental errors within ± 0.005. Therefore the Ti^{3+} ions are estimated to be up to $\sim$1–2% of all the Ti ions. For convenience, the samples will be denoted $Ln_{2/3}TiO_3$ for most of the discussion hereafter.

DC magnetization measurements were performed using a SQUID magnetometer (Quantum Design MPMS-XL5). Susceptibility–temperature (χ–T) curves were measured between 2 and 300 K in field-cooled (FC) and zero-field-cooled (ZFC) modes with an applied field (H) up to 10000 Oe. After the sample was heated, the curves were also measured using magnetization–applied field ($M - H$) curve measurements at 2 K, which will be denoted the MH mode hereafter.

3. RESULTS AND DISCUSSION

Figure 1a shows the XRD patterns for $Pr_{2/3}TiO_3$ prepared in the H_2–Ar flow at 1400°C, where only the Bragg peaks of the reaction product are observed. This pattern is almost the same as that of a slightly oxygen-deficient compound $La_{2/3}TiO_{2.970}$, which was assigned to the double perovskite structure of the orthorhombic space group *Pmmm* (6). A peak at $2\theta \sim 11^\circ$ reveals the double structure arising from the crystallographic ordering of the *A*-site vacancy (5,6). Indeed the present pattern could be fitted to this symmetry with parameters similar to those given to $La_{2/3}TiO_{2.970}$. The fitting parameters and reliability factors are shown in Table 1. The occupancies for *Ln*1 and *Ln*2 were determined on the condition of their sum being equal to the stoichiometric value. It is relevant that most of the parameters are quite close to those of $La_{2/3}TiO_3$. The smaller cell volume (V) than that of $La_{2/3}TiO_3$ ($a = 3.8789$ Å, $b = 3.8668$ Å, $c = 7.7866$ Å, $V = 116.79$ Å^3 (6)) is obviously due to the lanthanide contraction. Figure 1b shows the XRD pattern for the sample fired in air at 1400°C. Apparently this complex pattern cannot be regarded as that of any single-phase compound, which indicates that $Pr_{2/3}TiO_3$ can be synthesized only in a reducing atmosphere as in the case of $La_{2/3}TiO_3$ (5,6). Patterns analogous to those in Fig. 1b were observed, even when the firing temperature was raised to 1450°C, where the initial mixtures were found to melt. Although the quenching of the initial mixtures down to room temperature was also attempted in order to obtain any single-phase compound, the results were essentially the same as those in Fig. 1b.

Figure 1c shows the XRD patterns for $Nd_{2/3}TiO_3$ prepared in H_2–Ar flow at 1450°C. This pattern could be well fitted in the same manner used for $Pr_{2/3}TiO_3$. The results of the Rietveld analysis are displayed in Table 1. The *a*- and *b*-lengths are smaller than those of $Pr_{2/3}TiO_3$, while the *c*-length is slightly larger. The change in the unit cell volume V follows the lanthanide contraction. Also, this compound could not be synthesized in air, resulting in XRD patterns analogous to those in Fig. 1b.

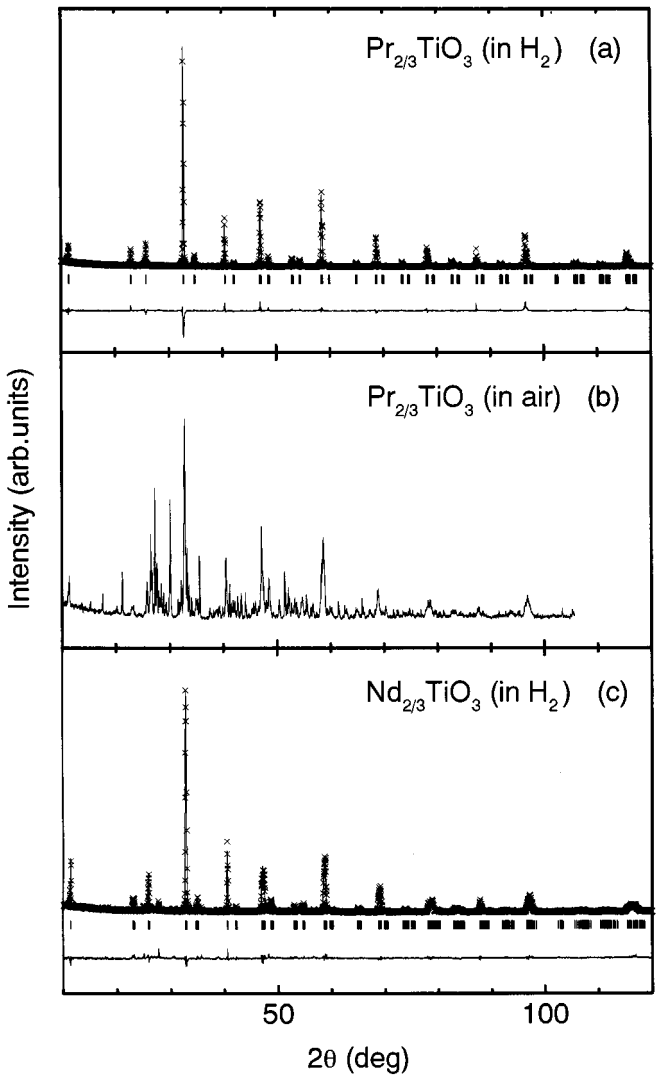

FIG. 1. XRD patterns for (a) $Pr_{2/3}TiO_3$ prepared in an H_2–Ar flow, (b) $Pr_{2/3}TiO_3$ fired in air, and (c) $Nd_{2/3}TiO_3$ prepared in an H_2–Ar flow. In (a) and (c), the X's and solid lines in the top stand for the observed and calculated patterns, respectively. The vertical lines in the middle indicate the Bragg angles calculated. The lower solid lines represent the differences between the observed and calculated patterns.

Although the synthesis of $Sm_{2/3}TiO_3$ in an H_2–Ar flow was investigated as well, the XRD patterns were not the same as those of $Pr_{2/3}TiO_3$ and $Nd_{2/3}TiO_3$. Its actual oxygen content was the same as that for $Pr_{2/3}TiO_3$ and $Nd_{2/3}TiO_3$. The XRD pattern is shown in Fig. 2. Impurity peaks below 30° could not be removed even when the firing temperature was raised to 1450–1500°C. The angles and intensities of the Bragg peaks, except those of the impurity, are close to these for a pyrochlore titanate $Sm_2Ti_2O_7$ (cubic *Fd3m*, $a = 10.23$ Å) (10). Indeed, the Rietveld analyses for this pattern led to a cubic symmetry of $a = 10.2026(3)$ Å

TABLE 1
Results Obtained from the Rietveld Analyses for $Pr_{2/3}TiO_3$ and $Nd_{2/3}TiO_3$

Atom	Occupation	x	y	z
Orthorhombic $Pr_{2/3}TiO_3$ (space group *Pmmm*)				
$a = 3.8582(1)$ Å, $b = 3.8644(2)$ Å, $c = 7.7335(4)$ Å, $V = 115.30$ Å^3				
$R_{WP} = 18.11\%$, $R_1 = 13.30\%$, $R_F = 7.91\%$				
*Ln*1	0.430	0	0	0.5
*Ln*2	0.904	0	0	0
Ti	1	0.5	0.5	0.2630(7)
O1	1	0.5	0.5	0.5
O2	1	0	0.5	0.2009(20)
O3	1	0.5	0	0.2962(21)
O4	1	0.5	0.5	0
Orthorhombic $Nd_{2/3}TiO_3$ (space group *Pmmm*)				
$a = 3.8336(2)$ Å, $b = 3.8520(2)$ Å, $c = 7.7413(4)$ Å, $V = 114.3$ Å^3				
$R_{WP} = 15.36\%$, $R_I = 5.99\%$, $R_F = 4.50\%$				
*Ln*1	0.404	0	0	0.5
*Ln*2	0.930	0	0	0
Ti	1	0.5	0.5	0.2623(5)
O1	1	0.5	0.5	0.5
O2	1	0	0.5	0.2164(10)
O3	1	0.5	0	0.2717(17)
O4	1	0.5	0.5	0

Note. The occupancies for *Ln*1 and *Ln*2 were determined on the condition of their sum being equal to the stoichiometric value. Their deviations are ~ 0.01. Isotropic parameters (B) were fixed at 0.3 Å^2.

with reliability factors up to $\sim 16\%$, assuming an oxygen stoichiometric $Sm_2Ti_2O_7$ phase since a slight oxygen deficiency hardly affects the analyses. Therefore the impurity phase is ascribed as excess titanium oxides. This result reveals that the $Ln_{2/3}TiO_3$ phase is not stable with $Ln = Sm$, and phase separation occurs instead. For this system, the same XRD patterns were obtained when the firing was done in air up to 1450°C.

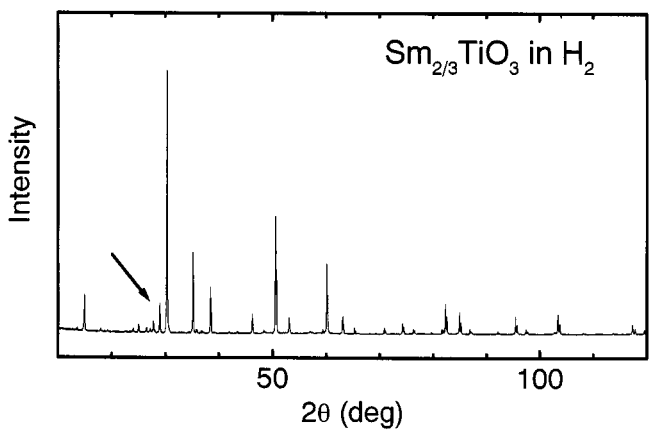

FIG. 2. XRD patterns for $Sm_{2/3}TiO_3$ prepared in an H_2–Ar flow. Several weak peaks pointed to by the arrow are from impurity phases.

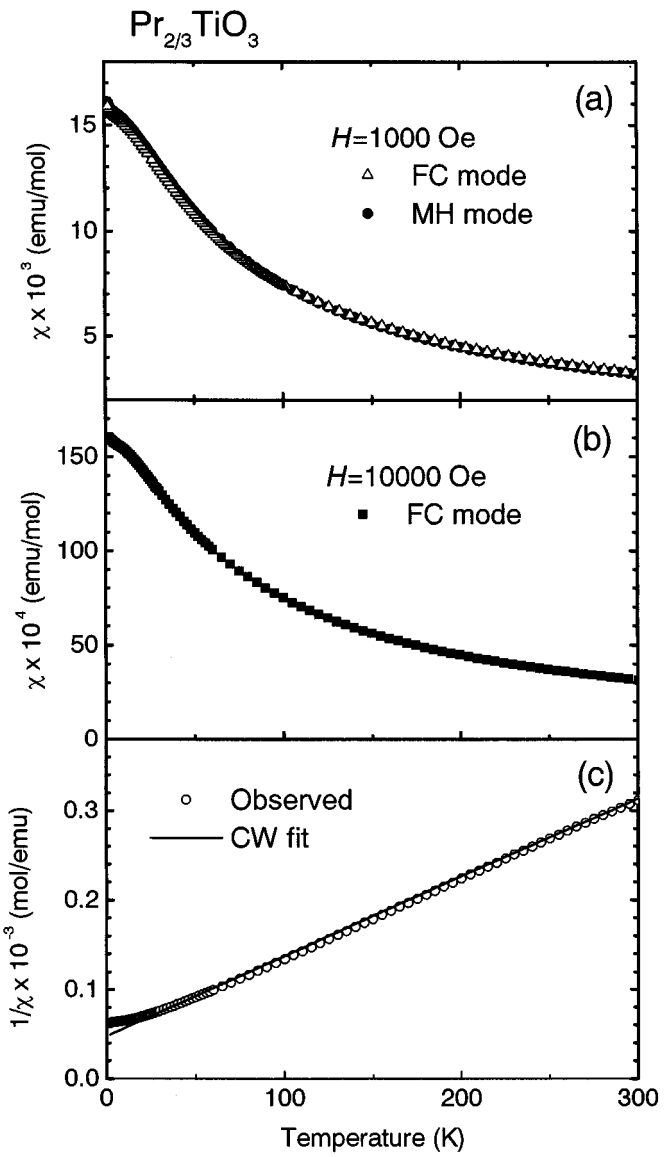

FIG. 3. (a) The χ–T curves for $Pr_{2/3}TiO_3$ measured with the applied field $H = 1000$ Oe. (b) The FC χ–T curve for $H = 10000$ Oe. (c) The $1/\chi$–T curve derived from the data in (a), denoted observed; the solid line stands for the result of Curie–Weiss (CW) fitting.

Figure 3a shows χ–T curves for $Pr_{2/3}TiO_3$, measured in the FC and MH modes with the applied field $H = 1000$ Oe. The two curves are almost the same, with no apparent magnetic ordering, which was true also for the ZFC mode. These curves were also measured with the applied fields $H = 100$ and 10000 Oe, and the features were essentially the same (Fig. 3b). Most of the Ti ions are in the diamagnetic Ti^{4+} ($3d^0$) state in this system. Based on the TGA analyses, the temperature dependence of the susceptibilities is due to the Pr^{3+} ($4f^2$) moments.

Figure 3c shows an inverse susceptibility–temperature ($1/\chi$–T) curve with $H = 1000$ Oe. The linear region above ~ 30 K was expressed in terms of the antiferromagnetic Curie–Weiss (CW) law, $1/\chi = (T + \Theta)/C$ with an effective localized moment 3.62 μ_B/Pr as shown in the figure. This is the same value as that of the free Pr^{3+} ion, which involves influences from thermally activated excited states (11). The result almost did not vary when the influence of the Ti^{3+} moments was included. In some perovskite oxides, the localized moments were reported to be slightly smaller than that of the free ion value due to the crystal field (12). For a comparably similar perovskite $PrScO_3$, where the magnetic ions are only in the lanthanide site, this value is calculated as 3.27 μ_B/Pr (12). Also, for some other oxide systems, they were found to be $\sim 10\%$ less than those of the free ions (12). The present result means that the crystal field hardly affects the ionic state of Pr^{3+} in $Pr_{2/3}TiO_3$. As the distances between the lanthanide and oxygen ions were not given for the above systems, detailed discussions of them do not seem to be warranted here. In comparison with that for $PrScO_3$, this result might be related to the weakening of the crystal field of oxygen due to the enhancement of the unit cell volume.

The upward deviation of the $1/\chi$–T curve from the CW fitting curve below $= 30$ K is characteristic in the figure, which indicates the decrease of a magnetic moment per unit formula. No suitable curve fitting was obtained, though the decrease of thermal excitation was taken into account where the decrease was essentially brought about by additional $\exp(-E/k_B T)$ terms (E, energy of excited states) (11). This was true when crystal field effects were considered. In addition, the crystal field effects cannot explain the free Pr^{3+} moment above ~ 30 K noted before. The fitting including the influences of the Ti^{3+} moments (effective moment 1.73 μ_B) exhibited slight downward deviation of the inverse susceptibilities in the case of both free Ti^{3+} moments and interacting Ti^{3+} moments with Pr^{3+}, assuming a Ti^{3+}–Pr^{3+} interaction similar to the Ti^{3+}–Gd^{3+} interaction for a perovskite titanate $GdTiO_3$ (13). At present the result is ascribed to the tendency toward antiferromagnetic ordering. Although M–H curves measured at 2, 5, and 10 K revealed paramagnetic profiles in the region up to 50,000 Oe (see Fig. 3), temperature derivatives of all the $1/\chi$–T curves were found to take minimums at 5–7 K, which implies the existence of magnetic ordering.

The value of Θ was calculated to be 52 K. This is considerably larger than that for $PrScO_3$, 8 K (12). This value is proportional to $zJ\mu^2$ where z, J, and μ stand for a coordination number, exchange interactions including that between the nearest neighbor ions, and an effective moment. This result means a considerably larger J value in the present system, considering that the z is roughly 2/3 times as large as that of $PrScO_3$, though the origin of this difference is ambiguous. In another similar perovskite, $NdScO_3$, a considerably similar value, 32 K, was obtained (12). Close values were also found for $PrTiO_3$ (49 K (12)) and $Nd_{1-x}TiO_3$ ($\sim$45–76 K, $x = 0$, 0.05, and 0.1 (14)), though the Ti^{3+} moments might play an important role in these systems. These values obtained from the CW fitting noted above were the same also in the case of the data with $H = 100$ and 10,000 Oe.

Figure 4 shows M–H curves measured at 2, 5, and 10 K. It is readily seen that all the curves exhibit only paramagnetic linear profiles up to 50,000 Oe. Therefore, to see whether magnetic ordering occurs as suggested by the derivatives of the $1/\chi$–T curves noted earlier, measurements at lower temperatures should be carried out in the future.

Figure 5a shows χ–T curves for $Nd_{2/3}TiO_3$ measured with $H = 1000$ Oe. As in the case of $Pr_{2/3}TiO_3$, the two curves are nearly the same, with no obvious magnetic ordering. The features of the curves were confirmed to be the same as those of the ZFC curve and of the curves measured with $H = 100$ and 10000 Oe. Figure 5b shows a $1/\chi$–T curve with $H = 1000$ Oe. The linear region above ~ 90 K was fitted also to the antiferromagnetic CW law with the same effective localized moment as that of the free Nd^{3+} ion, 3.68 μ_B (11). For $NdScO_3$, the value calculated from the C value is 3.48 μ_B, which is smaller that the free ion value due to the crystal field effects (12). Therefore the lanthanide ions are nearly in the free ionic state also in the present system. The influence of the Ti^{3+} moments hardly affected the fitting procedure as in $Pr_{2/3}TiO_3$. The obtained Θ value, 60 K, is slightly larger than that for $Pr_{2/3}TiO_3$ and $NdScO_3$ noted before. In comparison with $Pr_{2/3}TiO_3$, this is qualitatively explained in terms of both the larger localized moment of Nd^{3+} and the enhancement of magnetic interactions attributed to the shortening of the lanthanide ion distances in the a–b plane (see Fig. 1 in Ref. (6)).

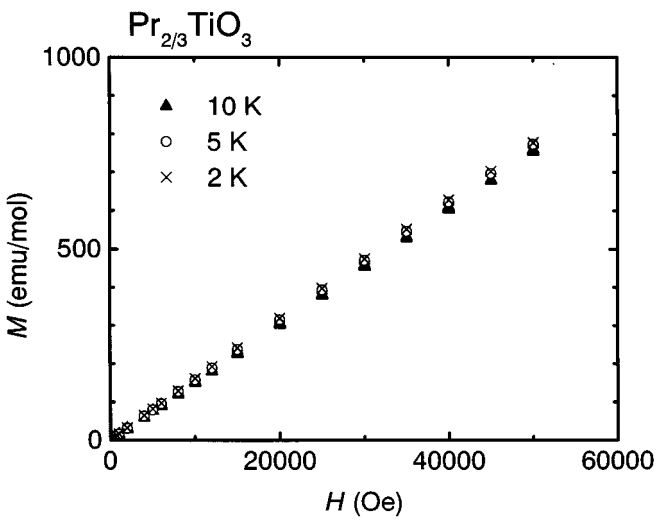

FIG. 4. M–H curves for $Pr_{2/3}TiO_3$ measured at 2, 5, and 10 K.

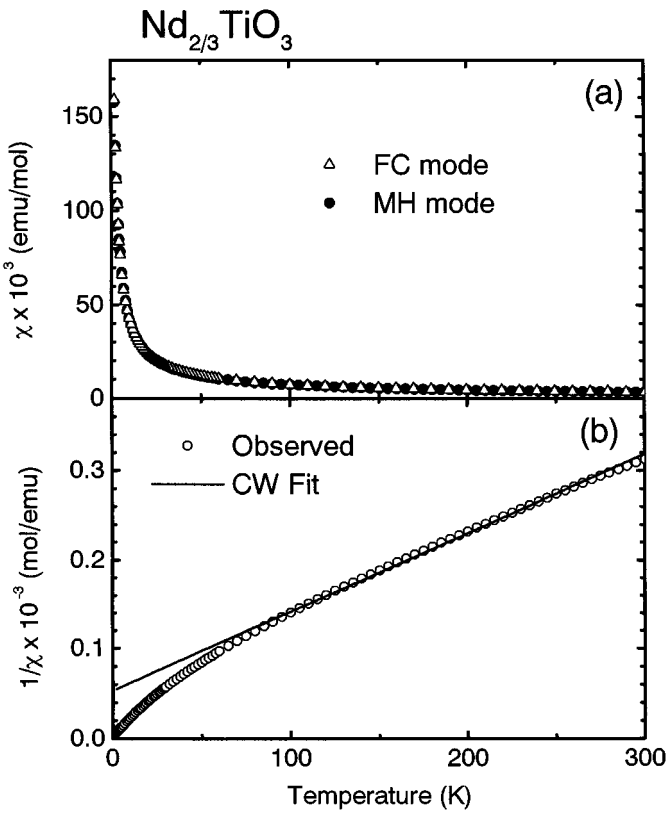

FIG. 5. (a) The χ–T curves for $Nd_{2/3}TiO_3$ measured with the applied field $H = 1000$ Oe. (b) The $1/\chi$–T curve derived from the data in (a), denoted observed; the solid line stands for the result of Curie–Weiss (CW) fitting.

This curve exhibits downward deviation of the inverse susceptibilities from the CW law below $\sim$90 K, which is apparently the reverse of the situation for $Pr_{2/3}TiO_3$. It is interesting that an analogous deviation was reported also for $NdScO_3$ below $\sim$60 K (12). This profile seems to be similar to that observed for ferrimagnetic ordering, which is expressed in terms of a four-parameter hyperbola (13). It was found that although this phenomenological model could be roughly fitted to the present data, it provided unreasonably large magnetic interactions between the Nd^{3+} ions larger than several hundred Kelvin, which was true also taking into account the Nd^{3+}–Ti^{3+} interaction. Though there exists no suitable fitting result for this deviation, the data plausibly suggest magnetic ordering at low temperatures.

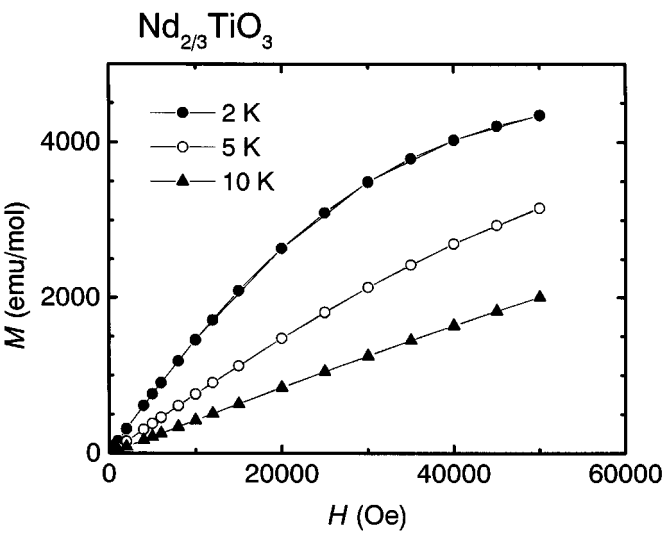

FIG. 6. M–H curves for $Nd_{2/3}TiO_3$ measured at 2, 5, and 10 K.

Figure 6 shows M–H curves at 2, 5, and 10 K for $Nd_{2/3}TiO_3$. The curve at 10 K is apparently almost paramagnetic. It is seen that the curve at 5 K exhibits very slight curvature. This curvature is much clearer in the 2 K curve, and the magnetization tends to saturate at high applied fields. This result is obviously different from that for $Pr_{2/3}TiO_3$ (Fig. 3) and implies the emergence of magnetic ordering at low temperatures. Therefore the deviation from the CW law is attributed to magnetic ordering. As temperature derivatives of the $1/\chi$–T curves exhibited no obvious minimum or maximum at all the temperatures, it is necessary to carry out the magnetization measurements at lower temperatures. Measurements are also required for $Pr_{2/3}TiO_3$ to clarify some of the ambiguous points noted above.

4. SUMMARY

The A-site-deficient perovskite compounds $Ln_{2/3}TiO_3$ with Ln = Pr and Nd were synthesized under an H_2–Ar atmosphere at 1400 and 1450°C, respectively. No single-phase compound could be prepared in air from the same initial mixtures. Their crystal structures were assigned to a double perovskite structure with the orthorhombic space group $Pmmm$, as in the case of $La_{2/3}TiO_3$. In both systems, no obvious magnetic ordering was observed between 2 and 300 K in the χ–T curves. The $1/\chi$–T curves were found to deviate from the Curie–Weiss law below $\sim$30 and $\sim$90 K for $Pr_{2/3}TiO_3$ and $Nd_{2/3}TiO_3$, respectively. The M–H curves exhibited paramagnetic profiles for $Pr_{2/3}TiO_3$ down to 2 K and a tendency of magnetic ordering for $Nd_{2/3}TiO_3$ at 2 K.

REFERENCES

1. D. Ridgly and R. Ward, *J. Am. Ceram. Soc.* **77,** 6132 (1955).
2. E. J. Hubibregtse, D. B. Barker, and G. C. Danielson, *Phys. Rev.* **82,** 770 (1951).
3. H. P. Rooksby, E. A. D. White, and S. A. Lanston, *J. Am Ceram. Soc.* **48,** 447 (1965).
4. P. N. Iyer and A. J. Smith, *Acta Cystallogr.* **23,** 740 (1967).
5. M. Abe and K. Uchino, *Mater. Res. Bull.* **9,** 147 (1974).

6. I.-S. Kim, T. Nakamura, Y. Inaguma, and M. Itoh, *J. Solid State Chem.* **113,** 281 (1994).
7. M. Yokoyama, T. Ota, I. Yamai, and J. Takahashi, *J. Cryst. Growth* **96,** 490 (1989).
8. Y. Okada, T. Arima, Y. Tokura, C. Murayama, and N. Mori, *Phys. Rev. B* **48,** 9677 (1993).
9. F. Izumi, "The Rietveld Method" (R. A. Young, Ed.), Oxford University Press, London, 1993; Y.-I. Kim and F. Izumi, *J. Ceram. Soc. Jpn.* **102,** 401 (1994).
10. Powder Diffraction File, Inorganic, 16-400, JCPDS-International Center for Diffraction Data: M. A. Subramanian, G. Aravamudan, and G. V. S. Rao, *Prog. Solid. State Chem.* **15,** 55 (1983).
11. For example, J. H. Van Vleck, "The Theory of Electric and Magnetic Susceptibilities." Oxford University Press, London, 1965.
12. D. A. MacLean, K. Seto, and J. E. Greedan, *J. Solid State Chem.* **40,** 241 (1982).
13. J. P. Goral and J. E. Greedan, *J. Solid State Chem.* **43,** 204 (1982).
14. G. Amow and J. E. Greedan, *J. Solid State Chem.* **121,** 443 (1996).